

Optical whirlpool on an absorbing metallic nanoparticle

M. V. Bashevoy, V. A. Fedotov and N. I. Zheludev

EPSRC NanoPhotonics Portfolio Centre, School of Physics and Astronomy, University of Southampton, SO17 1BJ, United Kingdom

bmv@soton.ac.uk

Abstract: The power-flow lines of light interacting with a metallic nanoparticle, in the proximity of its plasmon resonance, form whirlpool-like nanoscale optical vortices. These vortices were independently observed using analytical Mie theory and 3D finite element numerical modelling of the Maxwell equations. Two different types of vortex have been detected. The outward vortex first penetrates the particle near its centerline then, on exiting the particle, the flow-lines turn away from the centerline and enter a spiral trajectory. Outward vortices are seen for the wavelengths shorter than the plasmon resonance. For the wavelengths longer than the plasmon resonance the vortex is inward: the power-flow lines pass around the sides of the particle before turning towards the centerline and entering the particle to begin their spiral trajectory.

© 2005 Optical Society of America

OCIS codes: (260.5740) Physical Optics. Resonance.

References and links

1. J. R. Krenn, "Nanoparticle waveguides: watching energy transfer," *Nature Materials* **2**, 210–211 (2003).
2. M. L. Brongersma, J. W. Hartman, and H. A. Atwater, "Electromagnetic energy transfer and switching in nanoparticle chain-arrays below the diffraction limit," *Phys. Rev. B* **62**, R16356 (2000).
3. S. A. Maier, P. G. Kik, and H. A. Atwater, "Optical pulse propagation in metal nanoparticle chain waveguides," *Phys. Rev. B* **67**, 205402 (2003).
4. Special issue on singular optics, edited by M. V. Berry, M. Dennis, and M. Soskin, *J. Opt. A* **6**, (2004).
5. M. V. Berry, "Exuberant interference: Rainbows, tides, edges, (de)coherence," *Phil. Trans. R. Soc. Lond. A* **360**, 1023–1037 (2002).
6. H. F. Schouten, T. D. Visser, and D. Lenstra, "Optical vortices near sub-wavelength structures," *J. Opt. B* **6**, (2004).
7. H. F. Schouten, T. D. Visser, and G. Gbur, "Diffraction of light at slits in plates of different materials," *J. Opt. A* **6**, (2004).
8. G. Mie, "Beitrage zur optik truber medien, speziell kolloida ler metallosungen," *Ann. Physik* **25**, 377 (1908).
9. H. C. van der Hulst *Light scattering by small particles* (Wiley, New York, 1983).
10. J. V. Dave, "Scattering of electromagnetic radiation by a large, absorbing sphere," *IBM J. Res. Dev.* **13**, 302 (1969).
11. C. Sonnichsen, T. Franzl, and T. Wilk, "Plasmon resonances in large noble-metal clusters," *New. J. Phys.* **4**, 93.1–93.8 (2002).
12. J. R. Krenn, A. Dereux, and J. C. Weeber, "Squeezing the optical near-field zone by plasmon coupling of metallic nanoparticles," *Phys. Rev. Lett.* **82**, 2590–2593 (1999).
13. C. F. Bohren, and D. R. Huffman, *Absorption and Scattering of Light by Small Particles* (Wiley, New York, 1983).
14. H. Kuwata, H. Tamaru, K. Esumi, et. al., "Resonant light scattering from metal nanoparticles: Practical analysis beyond Rayleigh approximation," *Appl. Phys. Lett.* **83**, 4625 (2003).
15. *Handbook of chemistry and physics*, edited by R. Lide (CRC Press, New York, 2000).
16. J. L. Volakis, A. Chatterjee and L. C. Kempel, "Review of the finite element method for three-dimensional electromagnetic scattering," *J. Opt. Soc. Am. A* **11**, 1422 (1994).

17. J. Jin, *The Finite Element Method in Electromagnetics* (John Wiley and Sons, New York, 2002).
18. M. Dorobantu, "Efficient streamline computations on unstructured grids", Department of Numerical Analysis and Computing Science, Royal Institute for Technology, Stockholm (1997).
19. Z. B. Wang, B. S. Luk'yanchuk, M. H. Hong, et. al., "Energy flow around a small particle investigated by classical Mie theory," *Phys. Rev. B* **70**, 035418 (2004).

The structures of optical fields around metallic nano-particles are of special interest due to their role in nanophotonic and plasmonic devices and meta-waveguides [1, 2, 3]. Here we report that light interacting with an absorbing metallic nanoparticle follows curly trajectories with curvatures on the sub-wavelength scale, creating whirlpool-like nanoscale optical vortices. These "energy sink" vortices with spiral energy flow line trajectories are seen in the proximity of the nanoparticle's plasmon resonance.

Optical vortices have been identified as features in scalar wavefront dislocations of monochromatic light fields and modal lines corresponding to non-monochromatic light as well as in singularities in the maps representing vectorial properties of light [4]. It is now recognized that singularities are often features of fields near sub-wavelength structures. A vortex structure in the streamlines of the Poynting vector has been detected for Sommerfeld's edge diffraction with discussion of the eel-like motion of light at the edge dating back to Newtonian times [5]. Recently vortices were found in light diffracted by narrow slits in silver and silicon [6, 7]. However, to the best of our knowledge, optical whirlpool have never been studied in ellipsoidal and spherical metal nanoparticles.

We studied the interaction of light with homogeneous isotropic spherical nanoparticles using Mie theory and also solving the Maxwell equations numerically. The Mie theory [8] is an exact analytical wave theory giving time-harmonic electromagnetic fields \mathbf{E} and \mathbf{H} at frequency ω that satisfy the wave equations

$$\nabla^2 \mathbf{E} + k^2 \mathbf{E} = 0, \quad \nabla^2 \mathbf{H} + k^2 \mathbf{H} = 0, \quad (1)$$

where $k^2 = \omega^2 \epsilon \mu$. The solutions to these equations are presented in the form of a series of spherical Bessel functions inside the particle and spherical Hankel functions outside it (see Appendix). The nanoparticle is assumed to have a dielectric coefficient ϵ and permittivity μ . Mie theory gives exact solutions of the vector wave equation for the internal and scattered fields of the particle and has generated a massive body of literature in which field patterns for angle-dependant scattering, modes of excitation, and integral characteristics such as absorption and scattering cross-section have been calculated [9, 10]. The theory is still widely used in nanophotonics, particularly in cases involving single metallic nanoparticles [11] and nanoparticle waveguides [12]. It has been shown that light can bend near a nanoparticle [13], however it has never been determined that the interaction of light with a nanoparticle can create a nanoscale vortex field structure. Here we refer to vortices in the "trajectory" of light near the nanoparticle as defined by the lines of powerflow, i.e. lines to which the Poynting vector $\mathbf{P} = [\mathbf{E} \times \mathbf{H}]$ is tangential. In the vortex regime of propagation the lines of powerflow are wound around the nanoparticle to create a nanoscale "whirlpool", comparable in size to the particle itself, whereby light seems to pass through the particle several times over. The results for nanospheres were obtained and visualized in the Mathworks Matlab environment by plotting the streamlines $\mathbf{A}(t) = (x(t), y(t), z(t))$ of the Poynting vector field computed by integrating the differential equation: $d\mathbf{A}/dt = \mathbf{P}(\mathbf{A})$, where t is length of the path [18].

We found that the vortex regime occurs in metallic (e.g. silver) nanoparticles in the vicinity of the plasmon absorption resonance. We analyzed the field structure around a nanoparticle excited by a plane electromagnetic wave. To illustrate the vortex structures graphically, we plotted solutions in the plane of polarization of the incident light using powerflow lines and a

color scale for the absolute value of the Poynting vector (red = high, blue = low). In the field maps presented below the incident light is polarized in the plane of the page and propagates from left to right.

To relate the parameter field for our calculations to observable values we shall define the dimensionless scattering σ_s and absorption σ_a cross-sections of the nano-particle. In the Rayleigh approximation, cross-sections for a particle much smaller than the wavelength are introduced via the particle's polarizability α and its geometrical cross-section S : $\sigma_s = (k^4/6\pi)|\alpha|^2/S$ and $\sigma_a = k\text{Im}(\alpha)/S - \sigma_s$, where $k = 2\pi/\lambda$ is the wave vector, and polarizability is a function of the particle's shape and size [14].

We found that the existence of the vortex structure and the topography of the field maps depend on the values of the real and imaginary parts of the particle's complex dielectric coefficient $\epsilon = \epsilon' + i\epsilon''$ (see Fig. 2). Here and below we assume non-magnetic nanoparticles with $\mu = 1$. Figures 2(a) and (b) show the modification of the field structure around a hypothetical nanoparticle for different values of ϵ'' . In the case depicted in Fig. 2(a) the scattering and absorption cross-sections are much smaller than the geometrical cross-section and the particle is almost invisible to the external field ($\sigma_a = 0.47$, $\sigma_s = 0.03$). Most of the powerflow lines pass by the nanoparticle and only handful of them terminate on the particle, indicating small losses. In the case depicted in Fig. 2(b) the absorption cross-section approaches the plasmon resonance ($\sigma_a = 3.6$, $\sigma_s = 0.24$). Many flow-lines terminate at the nanoparticle (entering it from the front and the back, as in a similar case considered in [13]), indicating high losses. When the absorption and scattering cross-sections increase even further the flow lines create vortex-like structures around the nanoparticle. Figures 2(c) and (d) show such vortices around a silver nanoparticle at wavelengths of 354 nm (where $\epsilon = -2.0 + i0.28$, $\sigma_a = 5.8$ and $\sigma_s = 1.8$) and 367 nm (where $\epsilon = -2.71 + i0.25$, $\sigma_a = 4.1$ and $\sigma_s = 2.0$). These latter two pictures represent inward and outward vortices which lie in the plane of incident polarization. Our calculations show that in this central cross-section, light in the vortex remains linearly polarized in the plane of incidence. In the vortex regime the energy flow is dramatically disturbed in the vicinity of the particle. For the outward vortex, energy flow lines inside the particle go along the direction of the incident wave and are nearly parallel to it. Outside the particle energy moves in the opposite direction — the energy flow lines bend around the particle and re-enter it again. The situation is reversed for the inward vortex. Here, the energy flow inside the particle is in the direction opposite to the incident wave, while the energy flow outside the nanoparticle is mainly in the direction of the incident wave. In the plane perpendicular to the plane of polarization the powerflow lines exhibit no spiral features.

Figure 1 shows the parameter field where vortex structures can be observed. Two different types of vortex have been seen. In the first type, which we call an outward vortex, a bunch of powerflow lines first penetrate the particle near its centerline then, on exiting the particle, they separate, turn away from the centerline and enter a spiral trajectory. Outward vortices are seen to the “left” of the plasmon resonance i.e. for $\epsilon' > -2.2$ (in a spherical nanoparticle with a radius of 20 nm the plasmon resonance occurs at $\epsilon' \sim -2.2$). In the second type of vortex, which we call an inward vortex, the powerflow lines pass around the sides of the particle before turning towards the centerline and entering the particle to begin their spiral trajectory. Outward vortices are seen to the “right” of the plasmon resonance i.e. for $\epsilon' < -2.2$.

Although Mie theory is well established and trusted, its results are presented in polynomial form, bringing up the question of conversion. We therefore decided to verify the Mie theory results by comparing them with numerical solutions of the Maxwell equations. To analyze the vortex fields near spherical nanoparticles we used 64-bit software, developed by Comsol Inc., which implements a true 3D finite element method [16] and applies Perfectly Matched Layer (PML) [17] boundary conditions on all sides of the computational domain. We found that the

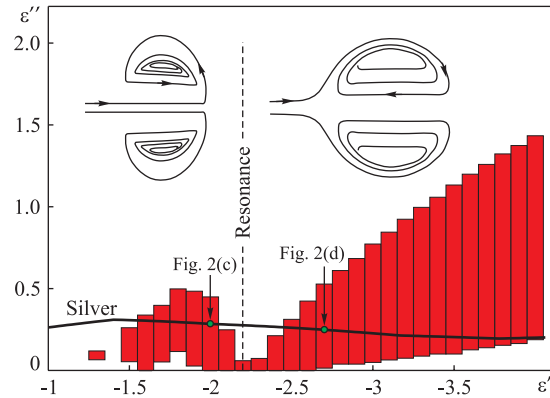


Fig. 1. Map showing values of the real and imaginary parts of the dielectric constant (in red) at which vortex field structures appear. The dashed line at $\epsilon' \sim -2.2$ indicates the position of the plasmon resonance in a spherical nanoparticle with $r \approx 20$ nm ($\lambda/r = 20$). The solid lines show the dispersion characteristics of the dielectric properties of silver.

analytical and numerical results correlated remarkably well, giving similar energy flow patterns.

Using the same numerical method we also found that vortex fields can exist near non-spherical nano-objects. Non-spherical nanoparticles are of considerable interest for applications because flattened or elongated shapes tend to reduce the plasmon resonance frequency, moving it from the blue-UV part of the spectrum to the more accessible visible-IR range. Mie theory is unsuitable for objects without spherical symmetry but computational methods provide an alternative to the analytical approaches and allow consideration of vortex fields around complex nanostructures. We investigated numerically a homogeneous oblate spheroidal nanoparticle with an aspect ratio of 2. Figure 3 shows the modification of the field structure around a spheroidal nanoparticle for different values of ϵ'' . Here again, one can see the weak interaction regime in Fig. 3(a) ($\sigma_a = 0.42$, $\sigma_s = 0.02$), the high-loss regime in Fig. 3(b) ($\sigma_a = 3.7$, $\sigma_s = 0.3$), the creation of outward vortices in Fig. 3(c) ($\sigma_a = 8.7$, $\sigma_s = 2.9$), and the creation of inward vortices in Fig. 3(d) ($\sigma_a = 2.9$, $\sigma_s = 1.3$).

There are a number of intriguing questions that may be asked in relation to the nanoscale structuring of the energy flow near and inside the nanoparticle. For instance, a vortex structure with light passing through a nanoparticle several times backwards and forwards, resembles a standing wave in a dissipative Fabry-Perot resonator. One may therefore wonder if such a “nano-resonator” could provide conditions for a hysteresis and bistability in the nanoparticle’s optical response if its dielectric properties depend on the intensity of light. The experimental observation of such hysteresis behavior would be clear evidence of the vortex energy flow. The existence of vortex structures in nanoparticles could provide a graphical interpretation of the fact that the absorption cross-section of a particle can be much bigger than its geometrical cross-section. When a vortex is created, powerflow lines pass through the nanoparticle several times, “multiplying” the light-matter interaction and generating the high energy losses associated with the large optical cross-section. Accurate phase and group delay measurements of light interacting with a nanoparticle near its plasmon resonance might provide further evidence for the long interaction time and thus for the existence of a vortex structure on the particle. At the stage of proofreading authors found a recent interesting publication devoted to complex patterns of energy flux in the near-field region around a small particle and the observation of energy flow “input windows” on the particle surface [19].

The authors would like to thank M. V. Berry for important comments and useful references

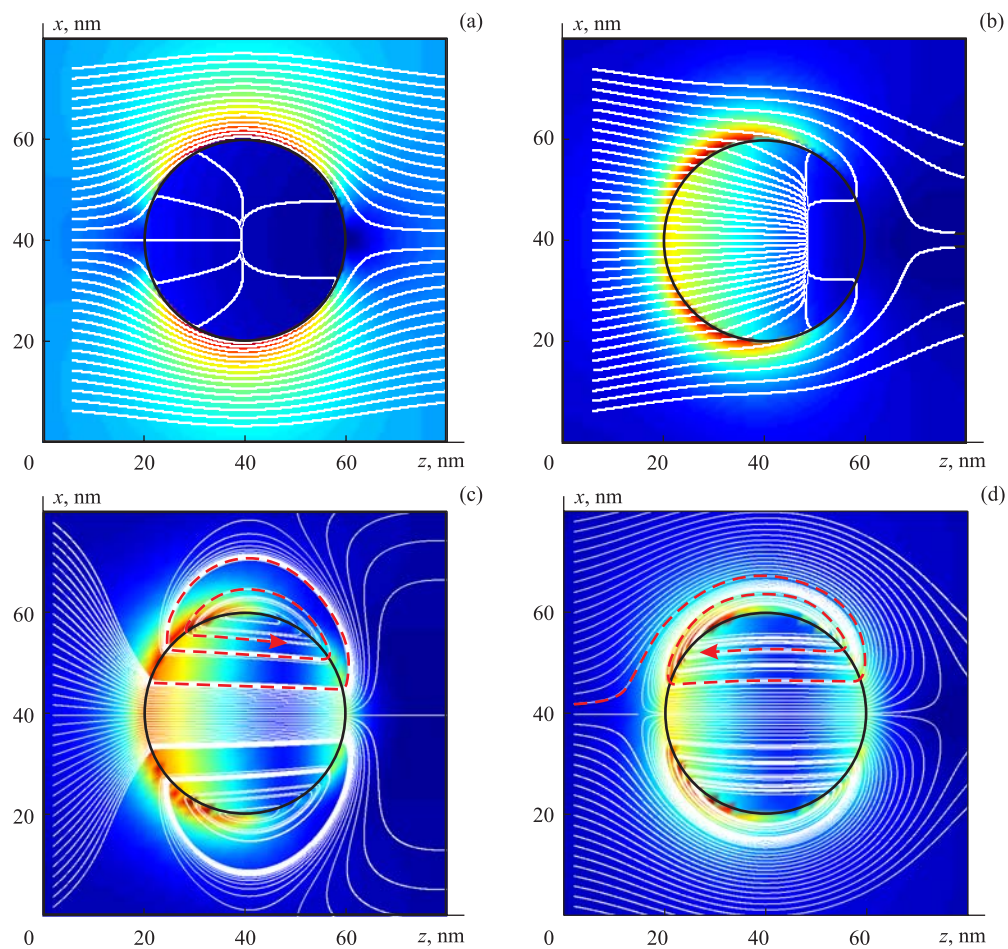


Fig. 2. [Movie 2.5 MB, 10.5 MB version] Mie Theory: powerflow distribution around a spherical nanoparticle with a radius of approximately 20 nm ($\lambda/r = 20$) in the plane containing the directions of propagation (from left to right) and polarization of the incident light. The colors indicate the absolute value of the Poynting vector, the white lines show the direction of powerflow. (a) $\epsilon = -2.0 + i10.0$, $\lambda = 400$ nm; (b) $\epsilon = -2.0 + i1.0$, $\lambda = 400$ nm; (c) $\epsilon = -2.0 + i0.28$ — the dielectric coefficient of silver at $\lambda = 354$ nm. Red dashed lines indicate outward vortex structure; (d) $\epsilon = -2.71 + i0.25$ — the dielectric coefficient of silver at $\lambda = 367$ nm. Red dashed lines indicate inward vortex structure [15].

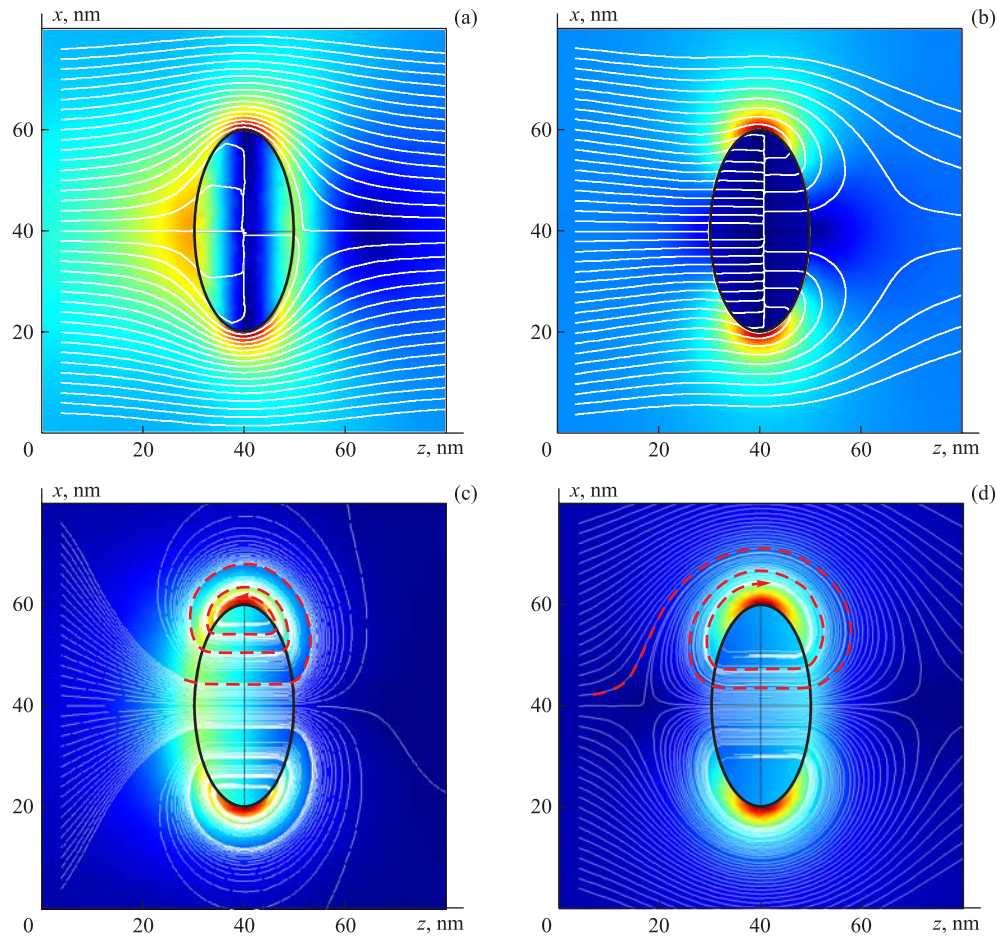


Fig. 3. 3D finite element modelling: powerflow distribution around an oblate spheroidal nanoparticle (with a semi-major axial radius of approximately 20 nm ($\lambda/r = 20$) and an aspect ratio of 2) in the plane containing the directions of propagation (from left to right) and polarization of the incident light. The colors indicate the absolute value of the Poynting vector, the white lines show the direction of powerflow. (a) $\epsilon = -3.52 + i10.0$, $\lambda = 400$ nm; (b) $\epsilon = -3.52 + i1.0$, $\lambda = 400$ nm; (c) $\epsilon = -3.37 + i0.2$ — the dielectric coefficient of silver at $\lambda = 380$ nm. Red dashed lines indicate outward vortex structure; (d) $\epsilon = -4.0 + i0.2$ — the dielectric coefficient of silver at $\lambda = 392$ nm. Red dashed lines indicate inward vortex structure [15].

and K. F. MacDonald for discussions and assistance with manuscript preparation and also to acknowledge the support of the Engineering and Physical Sciences Research Council (UK).

Appendix

Following [13] this Appendix shows the formulae used in the analytical Mie theory calculations of the internal and scattered fields of the metallic sphere. These fields and the incident field are presented in a spherical coordinate system with the polar axis directed along the incident light wave.

Incident field ($\mathbf{E}_i = E_0 e^{ikr \cos \theta} \mathbf{e}_x$):

$$E_{ir} = \sum_{n=1}^{\infty} E_n \left(-i \cos \phi n(n+1) \sin \theta \pi_n(\cos \theta) \frac{j_n(kr)}{kr} \right). \quad (2)$$

$$E_{i\theta} = \sum_{n=1}^{\infty} E_n \left(\cos \phi \pi_n(\cos \theta) j_n(kr) - i \cos \phi \tau_n(\cos \theta) \frac{[kr j_n(kr)]'}{kr} \right). \quad (3)$$

$$E_{i\phi} = \sum_{n=1}^{\infty} E_n \left(-\sin \phi \tau_n(\cos \theta) j_n(kr) + i \sin \phi \pi_n(\cos \theta) \frac{[kr j_n(kr)]'}{kr} \right). \quad (4)$$

$$H_{ir} = -\frac{k}{\omega} \sum_{n=1}^{\infty} E_n \left(i \sin \phi n(n+1) \sin \theta \pi_n(\cos \theta) \frac{j_n(kr)}{kr} \right). \quad (5)$$

$$H_{i\theta} = -\frac{k}{\omega} \sum_{n=1}^{\infty} E_n \left(-\sin \phi \pi_n(\cos \theta) j_n(kr) + i \sin \phi \tau_n(\cos \theta) \frac{[kr j_n(kr)]'}{kr} \right). \quad (6)$$

$$H_{i\phi} = -\frac{k}{\omega} \sum_{n=1}^{\infty} E_n \left(-\cos \phi \tau_n(\cos \theta) j_n(kr) + i \cos \phi \pi_n(\cos \theta) \frac{[kr j_n(kr)]'}{kr} \right). \quad (7)$$

Field inside the sphere:

$$E_{1r} = \sum_{n=1}^{\infty} E_n \left(-id_n \cos \phi n(n+1) \sin \theta \pi_n(\cos \theta) \frac{j_n(k_1 r)}{k_1 r} \right). \quad (8)$$

$$E_{1\theta} = \sum_{n=1}^{\infty} E_n \left(c_n \cos \phi \pi_n(\cos \theta) j_n(k_1 r) - id_n \cos \phi \tau_n(\cos \theta) \frac{[k_1 r j_n(k_1 r)]'}{k_1 r} \right). \quad (9)$$

$$E_{1\phi} = \sum_{n=1}^{\infty} E_n \left(-c_n \sin \phi \tau_n(\cos \theta) j_n(kr) + id_n \sin \phi \pi_n(\cos \theta) \frac{[k_1 r j_n(k_1 r)]'}{k_1 r} \right). \quad (10)$$

$$H_{1r} = -\frac{k_1}{\omega} \sum_{n=1}^{\infty} E_n \left(ic_n \sin \phi n(n+1) \sin \theta \pi_n(\cos \theta) \frac{j_n(k_1 r)}{k_1 r} \right). \quad (11)$$

$$H_{1\theta} = -\frac{k_1}{\omega} \sum_{n=1}^{\infty} E_n \left(-d_n \sin \phi \pi_n(\cos \theta) j_n(kr) + ic_n \sin \phi \tau_n(\cos \theta) \frac{[k_1 r j_n(k_1 r)]'}{k_1 r} \right). \quad (12)$$

$$H_{1\phi} = -\frac{k_1}{\omega} \sum_{n=1}^{\infty} E_n \left(-d_n \cos \phi \tau_n(\cos \theta) j_n(kr) + ic_n \cos \phi \pi_n(\cos \theta) \frac{[k_1 r j_n(k_1 r)]'}{k_1 r} \right). \quad (13)$$

Scattered field:

$$E_{sr} = \sum_{n=1}^{\infty} E_n \left(ia_n \cos \phi n(n+1) \sin \theta \pi_n(\cos \theta) \frac{h_n(kr)}{kr} \right). \quad (14)$$

$$E_{i\theta} = \sum_{n=1}^{\infty} E_n \left(-b_n \cos \phi \pi_n(\cos \theta) h_n(kr) + ia_n \cos \phi \tau_n(\cos \theta) \frac{[krh_n(kr)]'}{kr} \right). \quad (15)$$

$$E_{i\phi} = \sum_{n=1}^{\infty} E_n \left(b_n \sin \phi \tau_n(\cos \theta) h_n(kr) - ia_n \sin \phi \pi_n(\cos \theta) \frac{[krh_n(kr)]'}{kr} \right). \quad (16)$$

$$H_{ir} = \frac{k}{\omega} \sum_{n=1}^{\infty} E_n \left(ib_n \sin \phi n(n+1) \sin \theta \pi_n(\cos \theta) \frac{h_n(kr)}{kr} \right). \quad (17)$$

$$H_{i\theta} = \frac{k}{\omega} \sum_{n=1}^{\infty} E_n \left(-a_n \sin \phi \pi_n(\cos \theta) h_n(kr) + ib_n \sin \phi \tau_n(\cos \theta) \frac{[krh_n(kr)]'}{kr} \right). \quad (18)$$

$$H_{i\phi} = \frac{k}{\omega} \sum_{n=1}^{\infty} E_n \left(-a_n \cos \phi \tau_n(\cos \theta) h_n(kr) + ib_n \cos \phi \pi_n(\cos \theta) \frac{[krh_n(kr)]'}{kr} \right). \quad (19)$$

Where

$$a_n = \frac{m^2 j_n(mx) [xj_n(x)]' - j_n(x) [mxj_n(mx)]'}{m^2 j_n(mx) [xh_n(x)]' - h_n(x) [mxj_n(mx)]'}, \quad (20)$$

$$b_n = \frac{j_n(mx) [xj_n(x)]' - j_n(x) [mxj_n(mx)]'}{j_n(mx) [xh_n(x)]' - h_n(x) [mxj_n(mx)]'} \quad (21)$$

— coefficients inside the sphere.

$$c_n = \frac{j_n(x) [xh_n(x)]' - h_n(x) [xj_n(x)]'}{j_n(mx) [xh_n(x)]' - h_n(x) [mxj_n(mx)]'}. \quad (22)$$

$$d_n = \frac{mj_n(x) [xh_n(x)]' - mh_n(x) [xj_n(x)]'}{m^2 j_n(mx) [xh_n(x)]' - h_n(x) [mxj_n(mx)]'}. \quad (23)$$

— the scattering coefficients.

$$E_n = E_0 i^n (2n+1)/n(n+1).$$

$x = ka$ — size parameter, a — sphere radius, k — wavenumber of incident wave, $k_1 = mk$ — wavenumber inside the sphere, $m = \sqrt{\varepsilon}$ — relative refractive index, ε — dielectric constant of the sphere, ω — frequency of incident wave.

$$j_n(\rho) = \sqrt{\frac{\pi}{2\rho}} J_{n+1/2}(\rho) \text{ — spherical Bessel function, } J_{n+1/2}(\rho) \text{ — Bessel function.}$$

$$h_n(\rho) = \sqrt{\frac{\pi}{2\rho}} Y_{n+1/2}(\rho) \text{ — spherical Hankel function, } Y_{n+1/2}(\rho) \text{ — Hankel function.}$$

$$\pi_n = \frac{P_n^1}{\sin \theta}, \quad \tau_n = \frac{dP_n^1}{d\theta}, \quad P_n^1 \text{ — associated Legendre function.}$$